BIOCHEMISTRY

 Volume 46, Number 33 August 21, 2007

Articles

Unusual Structural Features of Hydantoin Lesions Translate into Efficient Recognition by *Escherichia coli* Fpg†

Nirmala Krishnamurthy,‡ James G. Muller,‡ Cynthia J. Burrows,‡ and Sheila S. David*,§

Department of Chemistry, University of California, One Shields Avenue, Davis, California 95616, and Department of Chemistry, University of Utah, 315 South, 1400 East, Salt Lake City, Utah 84112

Received November 29, 2006; Revised Manuscript Received April 20, 2007

ABSTRACT: Oxidation of guanine (G) and 8-oxoguanine (OG) with a wide variety of oxidants yields the hydantoin lesions, guanidinohydantoin (Gh) and spiroiminodihydantoin (Sp). These two lesions have garnered much recent attention due to their unusual structures and high mutagenic potential. We have previously shown that duplexes containing Gh and Sp are substrates for the base excision repair glycosylase *Escherichia coli* Fpg (EcFpg). To evaluate the recognition features of these unusual lesions, binding and footprinting experiments were performed using a glycosylase inactive variant, E3Q EcFpg, and 30 bp duplexes containing the embedded lesions. Surprisingly, E3Q EcFpg was found to bind significantly more tightly (~1000-fold) to duplexes containing Gh or Sp over the corresponding duplexes containing OG. This may be a consequence of the helix-destabilizing nature of the hydantoin lesions that facilitates their recognition within duplex DNA. Though DNA binding affinities of E3Q EcFpg with Gh- and Sp-containing duplexes were found to be similar to each other, hydroxyl radical footprinting using methidium-propyl-EDTA (MPE)-Fe(II) revealed subtle differences between binding of E3Q EcFpg to the two lesions. Most notably, in the presence of E3Q EcFpg, the Sp nucleotide (nt) is hyperreactive toward cleavage by MPE-Fe(II)-generated hydroxyl radicals, suggestive of the formation of an intercalation site for the MPE-Fe(II) reagent at the Sp nt. Interestingly, increasing the duplex length from 18 to 30 bp enhanced the excision efficiency of Gh and Sp paired with C, G, or T by EcFpg such that these substrates are processed as efficiently as the signature substrate lesion, OG. Moreover, the base removal activity with these two lesions was *more* efficient than removal of OG when in a base pairing context opposite A. The high affinity and efficient activity of EcFpg toward the hydantoin lesions suggest that EcFpg mediates repair of the lesions in vivo. Notably, the facile activity of EcFpg toward Gh and Sp in base pairing contexts with G and A, which are likely to be present after DNA replication, would be detrimental and enhance mutagenesis.

Reactive oxygen species (ROS),[1] such as superoxide, hydrogen peroxide, and hydroxyl radicals, are formed as byproducts of cellular metabolism or indirectly via external sources such as ionizing radiation (*1*, *2*). The presence of ROS can lead to various types of DNA damage, including strand breaks, protein−DNA cross-links, abasic sites, and

†This work was supported by a grant from the National Cancer Institute of the National Institutes of Health (CA90689).

* To whom correspondence should be addressed. Telephone: (530) 752-4830. Fax: (530) 752-8995. E-mail: david@chem.ucdavis.edu.

‡ University of Utah.

§ University of California.

10.1021/bi602459v CCC: $37.00
Published on Web 07/27/2007

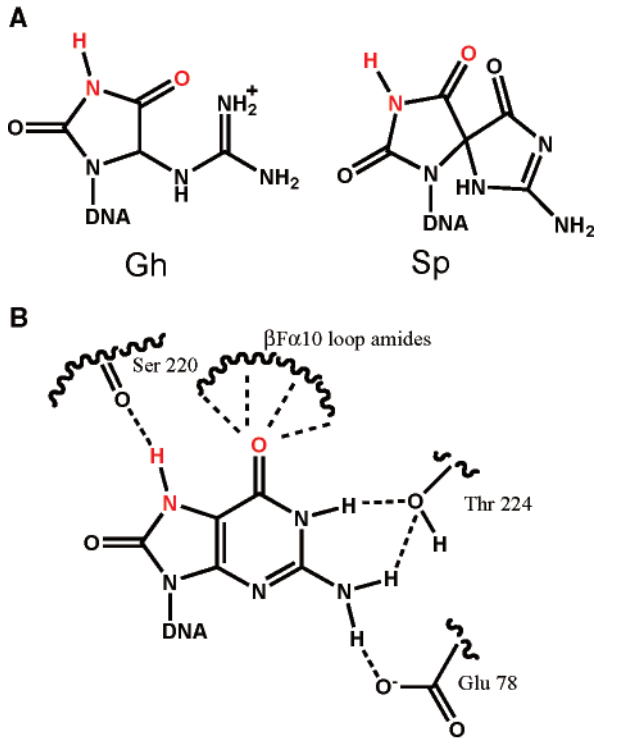

FIGURE 1: (A) Structures of guanidinohydantoin (Gh) and spiroiminodihydantoin (Sp) and (B) schematic of contacts made to 8-oxoguanine by E3Q BsFpg (*44*). (A) The hydantoin products Gh and Sp form from oxidation of OG or G with a variety of oxidants. Atoms that provide structural similarity to OG are colored red. (B) Residues and regions of the BsFpg enzyme that are involved in OG-specific contacts are indicated. The βFα10 loop refers to a loop that is ordered only in structures with the OG nt intact (*44*). There are many backbone amides (of residues 222−225 in βFα10) that are positioned in the proximity of O6 of OG. Atoms that provide OG-specific contacts with BsFpg are colored red. Note Fpg makes contacts to C that are not shown.

base lesions, which are potentially mutagenic and toxic to the cell (*1*, *3*−*5*). Fortunately, the integrity of DNA is preserved by a variety of DNA repair pathways (*6*−*9*). Indeed, defective DNA repair enzymes have been implicated in carcinogenesis, aging, and neurological disorders (*10*−*13*).

Much of the focus of oxidative base damage has been on an oxidation product of guanosine, 7,8-dihydro-8-oxo-2′-deoxyguanosine (OG), as the key biomarker of cellular oxidation (*4*, *14*, *15*). However, a wide variety of oxidized guanine lesions have been identified, resulting from either further oxidation of OG or direct oxidation of G (*16*). Of these further oxidized products, the hydantoin lesions, spiroiminodihydantoin (Sp) and guanidinohydantoin (Gh) (*17*, *18*) (Figure 1A), have interesting structural properties and have been identified as products in isolated DNA from oxidation of G and OG with a variety of oxidants, including singlet oxygen (*19*, *20*), type I photochemistry involving superoxide (*21*, *22*), high-valent chromium compounds (*23*, *24*), and peroxynitrite (*25*−*27*). The ability to form Sp and Gh under a variety of conditions is highly suggestive of their formation within cells. Indeed, recently, Sp was detected by ESI-MS in repair-deficient *Escherichia coli* that had been treated with chromate (*28*).

The hydantoin lesions have also been demonstrated to be highly mutagenic through both in vitro and in vivo studies. In single-nucleotide insertion and primer extension experiments using *E. coli* Klenow fragment of DNA polymerase lacking exonuclease activity (KF exo$^-$), dAMP and dGMP are inserted opposite these oxidized lesions (*29*, *30*). The response of DNA polymerases to OG is distinctly different with misinsertion of dAMP as well as correct insertion of dCMP to differing extents depending on the polymerase (*31*). However, in cellular experiments, OG is only mildly mutagenic, mediating G·C to T·A transversion mutations (~10%) (*32*, *33*). In contrast, in *E. coli*-based mutagenesis assays with a single-stranded lesion containing viral DNA, Gh and Sp are potently mutagenic (98%) causing both G → T and G → C transversion mutations (*34*, *35*).

Important features that influence the mutagenic potential of a given lesion is the efficiency of its repair, and the sensitivity of the repair enzymes to the correct base pairing context. The relatively low mutation frequency of OG, in both *E. coli* and mammalian cells, is due to efficient repair (*36*, *37*, *38*). The prevention of mutations associated with OG formed within duplex DNA in *E. coli* requires two base excision repair (BER) glycosylases MutM and MutY (*7*, *13*, *39*−*43*). *E. coli* MutM, also known as formamidopyrimidine glycosylase (EcFpg), removes OG from OG·C mispairs in the DNA duplex. Other enzymes of the BER pathway then act sequentially to restore the appropriate G·C base pair. Any OG·A base pairs formed during replication are intercepted by MutY which removes the inappropriately inserted adenine residues, thereby allowing re-creation of an appropriate OG·C substrate for EcFpg. Functionally similar BER glycosylases are also present in other organisms (*9*, *40*).

Structural studies of E3Q *Bacillus stearothermophilus* Fpg (BsFpg), a glycosylase inactive variant, bound to an OG·C substrate have illustrated features that allow for discrimination of OG from G (Figure 1B) (*44*). In addition to OG, Fpg has been shown to catalyze the removal of a variety of damaged bases, including ring-opened forms of purines such as 2,6-diamino-4-hydroxy-5-formamidopyrimidine (FapyG) and 4,6-diamino-5-formamidopyrimidine (FapyA), and oxidized pyrimidines such as 5-hydroxycytosine, 5-hydroxyuracil, and 5,6-dihydroxy-5,6-dihydrothymine (*40*). Previous work in our laboratory has shown that the hydantoin lesions, Gh and Sp, are also substrates for EcFpg (*45*), consistent with the retention of "OG-like" features in these lesions (Figure 1B). Gh and Sp lesions are also removed by endonuclease VIII (Nei) (*46*) and its mammalian counterparts, mNEIL1 and mNEIL2 (*47*). Surprisingly, Gh and Sp are not substrates for human OG glycosylase, hOGG1, though they are substrates for the homologous yeast OG glycosylases, yOGG1 and Ntg1 (*45*).

To further elucidate the features of recognition of the hydantoin lesions relative to OG by EcFpg, we analyzed the binding affinities of a glycosylase inactive variant E3Q

[1] Abbreviations: BsFpg, *Bacillus stearothermophilus* Fpg; BER, base excision repair; BSA, bovine serum albumin; DTT, dithiothreitol; EcFpg, *Escherichia coli* Fpg; EDTA, ethylenediaminetetraacetic acid; FapydG, 2,6-diamino-4-hydroxy-5-formamidopyrimidine; Fpg, formamidopyrimidine glycosylase or MutM; Gh, guanidinohydantoin; hOGG1, human OG glycosylase 1; IPTG, isopropyl β-D-thiogalactoside; nt, nucleotide; OG, 7,8-dihydro-8-oxoguanine; MPE, methidium-propyl-EDTA; PAGE, polyacrylamide gel electrophoresis; ROS, reactive oxygen species; Sp, spiroiminodihydantoin; TBE, tris-borate-EDTA; THF, tetrahydrofuran nucleotide; Tris, tris(hydroxymethyl)aminomethane; WT, wild type.

EcFpg (*44*) with 30 bp duplexes containing the embedded lesions. These studies reveal that E3Q EcFpg binds several orders of magnitude more tightly to duplexes containing Gh·C base pairs and Sp·C base pairs over the corresponding duplex containing OG·C base pairs. In addition, the higher affinity of E3Q EcFpg for Gh and Sp duplexes was observed when the lesions were positioned opposite C than G. Further subtleties in the properties of binding of E3Q EcFpg to Gh- and Sp-containing duplexes opposite both G and C were revealed using methidium-propyl-EDTA (MPE)-Fe(II) hydroxyl radical footprinting experiments. Indeed, the binding of EcFpg to Sp-containing duplexes creates a "hot spot" for intercalation at the Sp nucleotide. Interestingly, the use of the longer duplex substrates enhanced the efficiency of removal of Gh and Sp compared to that of the 18 bp duplex. In fact, within the longer duplex, the rate of removal of Gh and Sp opposite C, G, and T by EcFpg is similar to that for OG. However, when paired with A in both duplex lengths, EcFpg removes Gh and Sp more efficiently than OG. This work provides insight into features of these lesions that may lead to their efficient recognition and removal by EcFpg.

MATERIALS AND METHODS

General Materials and Instrumentation. 7,8-dihydro-8-oxo-2′-deoxyguanosine phosphoramidite was purchased from Glen Research. DNA oligonucleotides were synthesized according to the manufacturer's protocol on an Applied Biosystems model 392 DNA/RNA synthesizer. These samples were purified via HPLC on a Beckman Gold Nouveau system with a Protein-Pak DEAE 8HR column. Oligonucleotides used for mutagenesis via PCR were purified using oligonucleotide purification cartridges (OPC) from Perkin-Elmer. PCR was performed on a GeneAmp PCR 2400 system from Perkin-Elmer. Radiolabeling was conducted using [γ-^{32}P]-ATP purchased from GE Health Sciences with T4 polynucleotide kinase which was obtained from New England BioLabs. Labeled oligonucleotides were purified using ProbeQuant G-50 spin columns from GE Health Sciences according to the manufacturer's protocol. A Milli-Q PF system was used to purify distilled, deionized water that was used to make all the buffers. All buffers were passed through a 0.45 μm filter before they were used. Storage phosphor autoradiography was performed on a Typhoon 9400 phosphorimager system. Data analysis was performed using ImageQuaNT (version 5.2a), and the rate constants were determined from fitting of the data with GraFit 5.0. All other chemicals used for these experiments were purchased from Fisher Scientific, VWR, or Sigma.

Cloning of E3Q EcFpg. The "megaprimer"-based mutagenesis method (Stratagene) was used for site-directed mutagenesis according to the manufacturer's protocol. The necessary codon change that encodes the mutated enzyme E3Q EcFpg was incorporated into the *fpg* gene using the following primers: E3Q-1, 5′-GGAGATGCTATGCCT-CAATTACCCGAAGTTGAAACC-3′; E3Q-2, 5′-GGTTT-CAACTTCGGGTAATTGAGGCATAGCATCTCC-3′. The altered codon for mutagenesis of the appropriate amino acid is underlined. Plasmid DNA was isolated from XL-1 blue *E. coli* cells using a Wizard Plus DNA purification kit (Promega) according to the manufacturer's protocol. The presence of the correct mutation was confirmed by DNA sequencing provided by the core facility at the University of Utah Medical School.

Expression and Purification of WT and E3Q EcFpg. WT EcFpg was isolated using JM109 *E. coli* transformed with the pKKFapy2 overexpression plasmid (*48*). For E3Q EcFpg, the corresponding pKKFapy2 plasmid containing the altered *fpg* gene to produce the E3Q EcFpg protein, pKKE3Q, was transformed into competent CC104 *mutm*$^-$ cells. Cell growth, induction, and purification procedures for EcFpg and E3Q EcFpg were similar to those reported previously (*49*). The relevant concentrations of EcFpg or E3Q EcFpg were determined using the absorbance at 280 nm and the extinction coefficient ($\epsilon_{280} = 3.9 \times 10^4$ L mol^{-1} cm^{-1}). The active EcFpg concentration was determined as reported previously (*49*). An estimation of the amount of E3Q EcFpg protein competent for DNA binding (assuming a 1:1 binding stoichiometry) was determined using the Gh·C base pair-containing 30 bp duplex (*49*). This indicated only 7% of the sample was able to bind DNA, and therefore, all concentrations of E3Q Fpg were corrected using this value.

Substrate DNA Preparation. Gh- and Sp-containing nucleotides were synthesized from the original OG-containing nucleotides as previously described (*49*). The 30-nucleotide (nt) sequence that was used is d(5′-TGTTCATCATGGGTCX-TCGGTATATCCCAT-3′) in which X is OG, Gh, or Sp and the complementary strand d(3′-ACAAGTAGTACCCAGY-AGCCATATAGGGTA-5′) in which Y is C, A, T, or G. For all experiments, 2.5 pmol of the X-containing strand was radiolabeled on the 5′ end using [γ-^{32}P]ATP by T4 kinase at 37 °C. Excess [γ-^{32}P]ATP was removed using a GE Health Sciences Microspin G-50 spin column, according to the manufacturer's protocol. For the glycosylase activity assays, additional nonradioactive X-containing DNA was added to the labeled strand to allow 5% labeled DNA, which was then annealed to the complement (added at 20% excess) by heating it to 90 °C for 5 min and allowing it to cool overnight in annealing buffer [20 mM Tris-HCl (pH 7.6), 10 mM EDTA, and 150 mM NaCl]. For the binding affinity experiments, an equimolar amount of the complement was added to 100% radiolabeled X-containing DNA. The duplex was then annealed as described above. For binding experiments, the listed duplex concentrations are upper-limit values based on 100% assumed recovery after purification and labeling. For the footprinting experiments, either the X-containing or the Y-containing strand was radiolabeled according to the protocol for the binding affinity experiments described above.

Glycosylase Assays. Single-turnover experiments, where the enzyme concentration is greater than the DNA concentration, were performed using the 30 bp duplexes to evaluate the glycosylase activity of the enzymes. In each case, the total reaction volume was 60 μL with a final duplex DNA concentration of 20 nM. The duplex was incubated with 150−300 nM active Fpg in an assay buffer [20 mM Tris-HCl (pH 7.6), 10 mM EDTA, 0.1 mg/mL BSA, and 30 mM NaCl] at 37 °C. Aliquots were removed manually at various times (from 15 s to 60 min) and reactions quenched by the addition of 5 μL of 0.5 N NaOH. This was followed by the addition of 5 μL of formamide denaturing dye (80% formamide, 0.025% xylene cyanol, and 0.025% bromophenol blue in TBE buffer), and then the aliquots were heated to 90 °C for 2 min and placed on dry ice. The samples were

run on a 15% denaturing polyacrylamide gel in 1× TBE at 1600 V for 2 h. The separation of the 15 nt DNA fragment arising from the product and the 30 nt fragment originating from the substrate was visualized using autoradiography by exposure to a storage phosphor screen overnight. As a control, for several substrates that could be examined manually, parallel reactions of EcFpg with the substrates were quenched with NaOH or with formamide dye alone. Analysis of the extent of strand scission based on these experiments provided similar rates of reactions consistent with tight coupling of the glycosylase and lyase functions of EcFpg since the NaOH treatment would have cleaved any intact abasic sites. Control experiments without enzyme also established that the Gh and Sp lesions were cleaved minimally by the NaOH quenching (<5%). The extent of background cleavage due to the NaOH quenching was subtracted during quantitation of the storage phosphor autoradiograms.

For reactions in single-turnover experiments in which the glycosylase reaction was too fast to measure manually, a Rapid Quench Flow instrument (RQF-3) from Kintek was used. The reaction buffer and conditions and overall analysis are similar to those of the manual experiments. However, notably, addition of a nonspecific duplex (25 nM) to EcFpg (400 nM) while it was in the injection loop was found to be necessary to stabilize the enzyme. This particular ratio of DNA duplex to EcFpg provided optimal stability, without interfering with the reaction with the substrate duplex. Once mixed with the substrate DNA duplex, the final reaction concentrations were as follows: 20 nM substrate, 12.5 nM nonspecific DNA duplex, and 200 nM EcFpg. A water bath maintained the reaction temperature at 37 °C, and reaction mixtures were allowed to incubate for time points ranging from 0.1 s and 5 min before the reactions were quenched with 0.5 M NaOH. In all cases, the reported values are the average of at least three separate determinations, and the error is reported as the standard deviation of the sample set.

Equilibrium Dissociation Constant (K_d) Measurements. Electrophoretic mobility shift assays (EMSA) were performed to determine the K_d values. Reaction volumes contained 10 pM duplex DNA, 20 mM Tris-HCl (pH 7.5), 10 mM NaCl, 1 mM EDTA, 1 mM DTT, 10% glycerol, 0.1 mg/mL BSA, and E3Q Fpg concentrations ranging from 2 μM to 10 pM. Samples of the protein/DNA mixture were incubated at 25 °C for 30 min followed by the addition of 6 μL of nondenaturing loading dye (0.25% bromophenol blue, 0.25% xylene cylanol, and 30% glycerol in 1× TBE). Bound versus unbound DNA was resolved using electrophoresis on an 8% nondenaturing polyacrylamide gel (29:1 acrylamide: bisacrylamide ratio) at 4 °C in 0.5× TBE buffer at 120 V for 2 h. Gels were dried and exposed to a storage phosphor screen overnight. K_d values were determined by fitting the data (percent bound substrate vs enzyme concentration) using a one-site binding isotherm (GraFit 5.0).

MPE-Fe(II) Footprinting Experiments. Hydroxyl radical footprinting experiments using methidium-propyl-EDTA-Fe(II) [MPE-Fe(II)] were performed following the procedure previously reported by our laboratory (*50*). Briefly, reaction mixtures (10 μL) containing 10 nM 5′-end-labeled duplex DNA with the centralized lesion mispair and various amounts of E3Q Fpg (1−140 nM) were incubated in a buffer containing 10 mM Tris-HCl (pH 7.4), 10 mM NaCl, 0.1 μg/μL BSA, and 500 μM calf thymus DNA at 25 °C for 15 min. The MPE-Fe(II) solution was freshly prepared by mixing equal volumes of 1 mM MPE and 1 mM $Fe(NH_4)_2(SO_4)_2 \cdot 6H_2O$ followed by a 1:2 dilution in water. A 1:1 mixture of a MPE-Fe(II) solution and 10 mM sodium ascorbate (freshly prepared) was added (1 μL each) to the enzyme/DNA mixtures and then incubated at room temperature for 30 min. The reactions were quenched by adding 10 μL of formamide loading dye and the mixtures incubated at 90 °C for 3 min. Samples were then electrophoresed using a 15% denaturing acrylamide gel in 1× TBE buffer. Control reactions were also performed in the same way in the absence of E3Q Fpg and/or MPE-Fe(II).

Hydroxyl radical footprinting using Fe(II)-EDTA was performed on the E3Q Fpg complex with the Sp·G duplex in a manner analogous to that for MPE-Fe(II), except that 3 μL of a freshly prepared chilled solution containing 0.1% H_2O_2, sodium ascorbate (6.7 mM), and 0.1 mM $[Fe(EDTA)]^{2-}$ [0.2 mM $(NH_4)_2Fe(SO_4)_2 \cdot 6H2O$ and 0.4 mM EDTA] was added to each reaction mixture, instead of the MPE-Fe(II) solution.

RESULTS

EcFpg Exhibits a High Affinity for Gh- and Sp-Containing Duplexes. Measurements of dissociation constants (K_d) using electrophoretic mobility shift assays (EMSA) of WT EcFpg with substrates and abasic site product analogues have been reported previously (*51*−*55*). However, the reported K_d values with the substrates (*52*−*54*) are likely actually reporting the K_d values for dissociation of EcFpg from the product produced during the incubation of the enzyme with the substrate duplex prior to being loaded onto the gel. In fact, under appropriate K_d conditions, we observed significant amounts of conversion of the DNA substrate (e.g., Gh·C-containing duplex) to product at all concentrations of the enzyme titration (data not shown).[2] Thus, to evaluate recognition features of the hydantoin lesion substrates relative to OG without complications associated with the base cleavage reaction, a glycosylase inactive variant, E3Q EcFpg (*44*), was used. The EMSA experiments were performed using a 30 bp duplex ([DNA] < K_d) containing the oxidized lesion (OG, Gh, or Sp) base paired with C or G at 25 °C. In initial EMSA experiments, we attempted to use 18 bp duplexes containing Gh or Sp. However, with these duplexes, as the protein concentration was increased, single-stranded DNA was observed rather than the protein−DNA complex, suggesting that protein binding destabilizes the 18 bp duplex. For this reason, we turned to using a 30 bp duplex containing the same internal sequence as the 18 bp duplex used previously for kinetic studies. Representative plots of percent protein bound DNA versus E3Q EcFpg concentration from the EMSA experiments are shown in Figure 2, while K_d values determined from at least four different experiments are summarized in Table 1. As expected, E3Q EcFpg exhibits a higher affinity for the OG·C duplex (K_d of 280 ± 70 nM) than for a nonspecific duplex [K_d(est) > 2 μM]. However,

[2] Most glycosylases have a high affinity for the product, and in many cases, it is higher than that for the substrate. It should also be noted that many of the previous reports measured the K_d values using DNA concentrations that were close to K_d (i.e., too high), and this may contribute to inaccurate determinations of K_d.

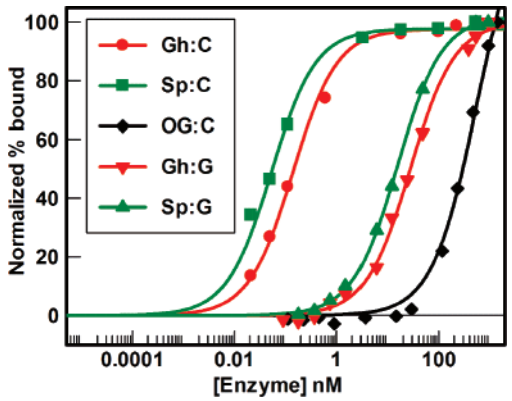

FIGURE 2: Representative data from an EMSA of binding of E3Q Fpg to OG-, Gh-, and Sp-containing 30 bp duplexes illustrating the relative affinity for the different lesions and changes with opposite base. Plot of percent E3Q Fpg bound to duplex containing a central OG·C (black diamonds), Gh·C (red circles), Sp·C (green squares), Gh·G (red inverted triangles) or Sp·G (green triangles) DNA as a function of E3Q Fpg concentration at 25 °C. Percent bound has been normalized to maximum amount of bound with a given duplex. Values determined from several experiments are listed in Table 1.

Table 1: Dissociation Constants (K_d[a]) for E3Q EcFpg with the 30 bp Duplex at 25 °C

central base pair	[E3Q Fpg] (nM)	central base pair	[E3Q Fpg] (nM)
OG·C	280 ± 70	Gh·G	25 ± 2
Gh·C	0.2 ± 0.1	Sp·G	15 ± 2
Sp·C	0.05 ± 0.02		

[a] Apparent K_d.

surprisingly, E3Q EcFpg binds with a significantly higher affinity to the Gh and Sp duplexes over the corresponding duplexes containing OG. The apparent dissociation constants observed with the duplex containing Gh·C (0.2 ± 0.1 nM) and Sp·C (0.05 ± 0.01 nM) base pairs are 2000- and 6000-fold higher, respectively, than that for the duplex containing the OG·C base pair. The binding of E3Q EcFpg is influenced by the base opposite the lesion as evidenced by the K_d values for the Gh·G and Sp·G base pair-containing duplex of 25 ± 2 and 15 ± 2 nM, respectively. These values are 200- and 400-fold greater than those for the corresponding duplex containing Gh·C and Sp·C base pairs, respectively.

Hydroxyl Radical Footprinting with MPE-Fe(II). Fe(II)-EDTA hydroxyl radical footprinting experiments with EcFpg bound to duplexes containing product analogues, such as THF, have been reported (*51*, *55*). In this work, we used MPE-Fe(II) to generate hydroxyl radicals, rather than Fe(II)-EDTA. With the MPE-Fe(II) reagent, the methidium intercalator delivers the Fe(II)-EDTA moiety to the double-helical regions of DNA, and therefore, deoxyribose cleavage by the generated hydroxyl radicals occurs more readily in regions of duplex DNA. The 30 bp duplex containing the oxidized lesions (Gh and Sp) paired with either C or G was incubated with increasing amounts of E3Q EcFpg followed by reaction with MPE-Fe(II). In each case, either the lesion-containing strand or the complementary strand had been 5′-end-labeled with ^{32}P-containing phosphate to allow for visualization. These strands were also subjected to the G+A Maxam−Gilbert reactions (*56*) to correlate the footprinted nucleotides surrounding the mispair to the sequence that was used.

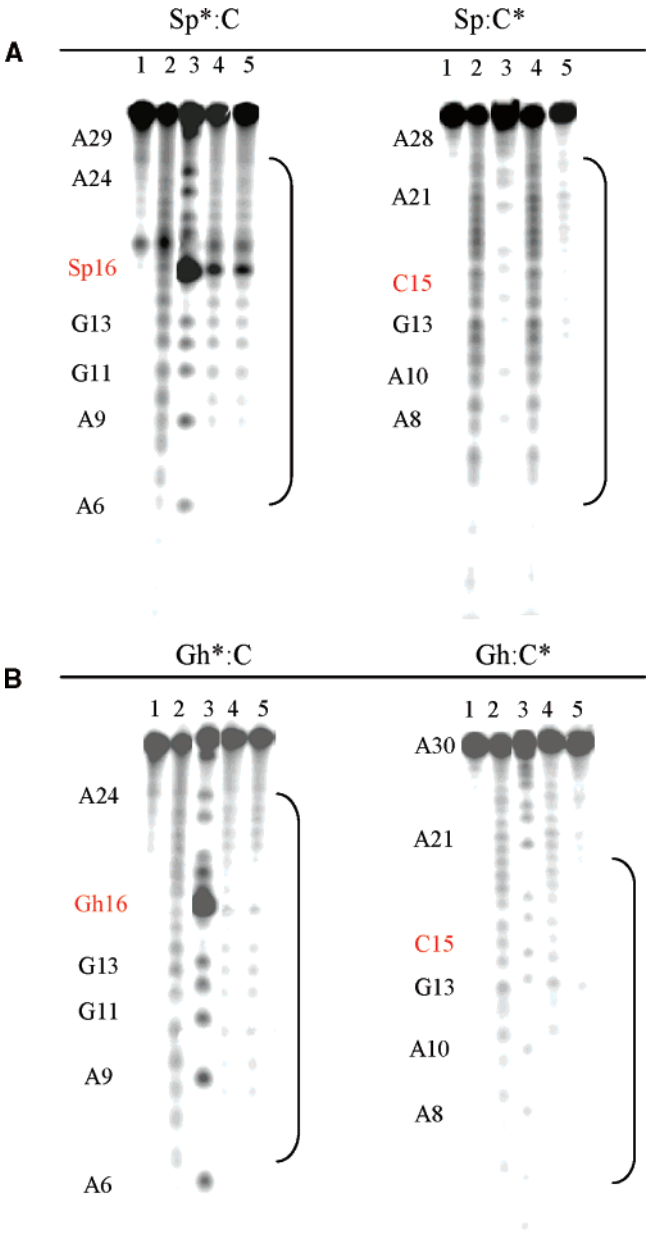

FIGURE 3: Storage phosphor autoradiogram of hydroxyl radical footprinting using MPE-Fe(II) of E3Q EcFpg with a 30 bp Sp·C and Gh·C duplex. The 30 bp DNA duplex containing the Sp·C mispair (A) or Gh·C mispair (B) was labeled at the 5′ end on either the Sp/Gh or C strand. The strand that is labeled in each case is denoted with an asterisk. The DNA was incubated at 25 °C under varying conditions: lane 1, no enzyme and no MPE-Fe(II) control; lane 2, no enzyme control; lane 3, G+A Maxam−Gilbert sequencing; lane 4, 3.5 nM E3Q EcFpg; and lane 5, 7 nM E3Q EcFpg. The position of the base pair, Sp·C or Gh·C, is highlighted in red. Brackets indicate protected regions on the DNA.

Representative storage phosphor autoradiograms of the footprinting experiments with E3Q EcFpg are shown in Figure 3. There is protection due to the presence of E3Q EcFpg on both strands of the DNA duplex. The amount of enzyme required for protection is different in each case and is consistent with the relevant dissociation constants (K_d) determined for each duplex (Table 1). It is also notable that we have been unable to observe a defined footprint with the OG·C duplex under our conditions. At concentrations where protection was observed, the entire duplex was protected rather than the just the OG·C base pair site. This suggests

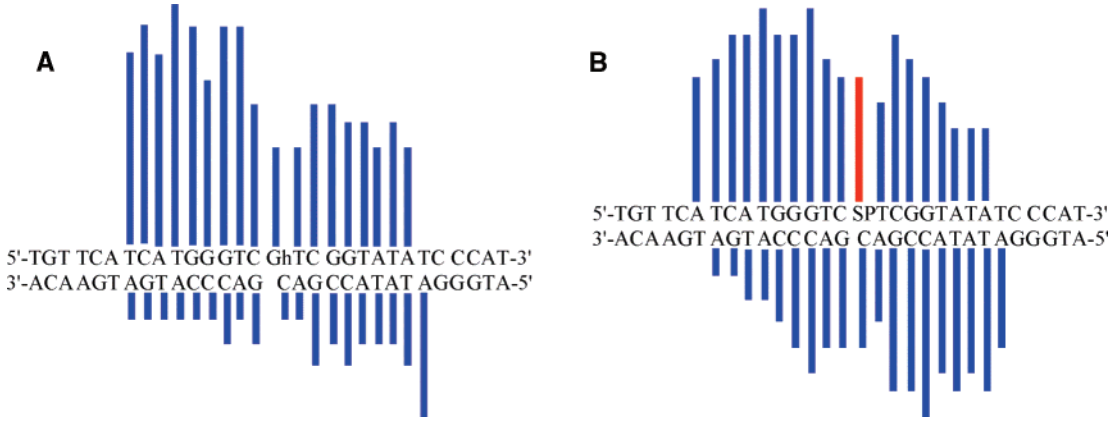

FIGURE 4: Hydroxyl radical footprinting using MPE-Fe(II) of E3Q EcFpg with Gh·C and Sp·C duplexes. Histograms of the hydroxyl radical footprinting with the 30 bp Gh·C (A) and Sp·C (B) duplexes illustrate the extent of protection from hydroxyl radical footprinting. The data were obtained by quantification of storage phosphor autoradiograms such as the one shown in Figure 3. The blue bars represent data for the footprinted nucleotides, while the red bar indicates data for a hyperreactive site. This histograms for Gh·C and Sp·C duplexes were determined from quantitation of the autoradiogram with an E3Q EcFpg concentration of 7 nM. For these two duplexes, the nucleotide with the maximum level of protection from the hydroxyl radical cleavage is taken as the standard and denoted by the highest bar. The extent of protection (or hyperreactivity) for the remaining nucleotides is depicted relative to this standard nucleotide. The absolute intensity of the cleavage at the Sp nucleotide in the presence of E3Q EcFpg is approximately 4-fold increased relative to the control without enzyme.

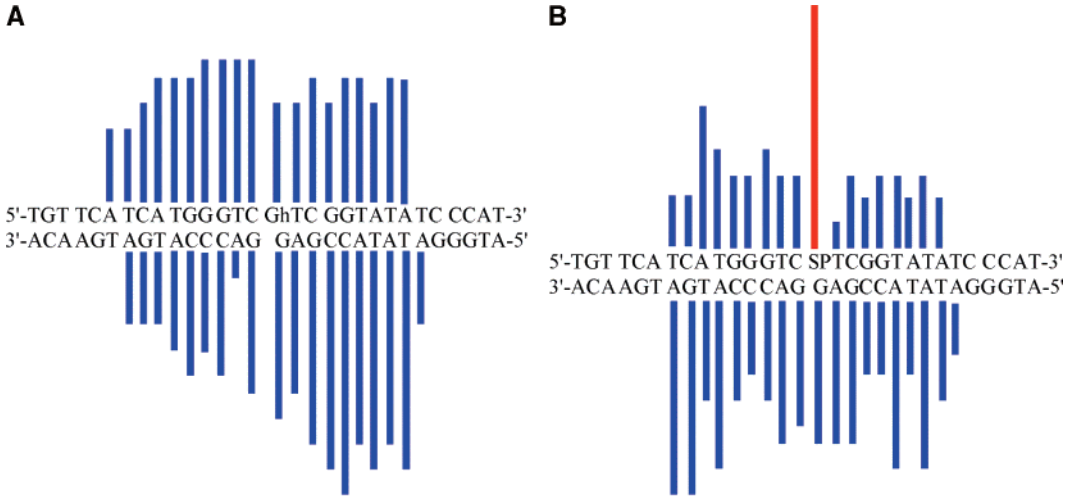

FIGURE 5: Hydroxyl radical footprinting using MPE-Fe(II) of E3Q EcFpg with Gh·G and Sp·G duplexes. Histograms of the hydroxyl radical footprinting with the 30 bp Gh·G (A) and Sp·G (B) duplexes illustrate the extent of protection from hydroxyl radical footprinting. The data were obtained by quantification of storage phosphor autoradiograms such as the one shown in Figure 3. The blue bars represent data for the footprinted nucleotides, while the red bar indicates data for sites of hyperreactivity. The histogram for the Gh·G and Sp·G duplexes is obtained at an E3Q EcFpg concentration of 70 nM. For these two duplexes, the nucleotide with the maximum level of protection from the hydroxyl radical cleavage is taken as the standard and denoted by the highest bar. The extent of protection or hyperreactivity for the remaining nucleotides is depicted relative to this standard nucleotide. The absolute intensity of the cleavage at the Sp nucleotide in the presence of E3Q EcFpg is approximately 4-fold increased relative to the control without enzyme.

that a larger difference in affinity, and more importantly enzyme off-rate, for the lesion site and the nonspecific duplex may be required for observation of a defined region of protection. This result is reminiscent of previous MPE-Fe(II) footprinting experiments with *E. coli* MutY where clear footprinted regions were observed in experiments with duplexes containing OG, but not G, opposite an abasic site or the 2′-deoxyadenosine analogue, 2′-deoxyformycin, despite the fact that MutY is competent at removing adenine when base paired with G and OG (*50*).

Representative histograms of the regions of the 30 bp DNA duplex surrounding the Gh and Sp opposite C or G protected by E3Q Fpg determined by quantitative analysis of the relevant storage phosphor autoradiograms are shown in Figures 4 and 5, respectively. The trends observed in each of the histograms are similar, and the protected region spans 15−16 nt on both strands of the DNA duplex. The footprinting experiments also reveal different patterns of protection of the duplexes containing Gh versus Sp. However, the most striking difference between the results with the Gh- and Sp-containing duplexes is the hyperreactivity of the Sp nucleotide to cleavage by MPE-Fe(II)-generated hydroxyl radicals in the presence of E3Q EcFpg (Figure 3A). The intensity of the cleavage observed at the Sp nt when paired with both G and C was increased approximately 4-fold in the presence of E3Q Fpg over the control with no enzyme.

To determine if the hyperreactivity of the Sp nt was related to the presence of the methidium intercalator, hydroxyl radical footprinting using Fe(II)-EDTA of E3Q EcFpg bound to an Sp·G base pair-containing duplex was performed. At

FIGURE 6: Relative extents of regions of DNA duplex protected by E3Q EcFpg using hydroxyl radical cleavage with Fe-EDTA (blue) vs MPE-Fe(II) (red).

Scheme 1

$$\text{Fpg} + (\text{DNA})_s \underset{k_{-1}}{\overset{k_1}{\rightleftharpoons}} \text{Fpg}\cdot(\text{DNA})_s \xrightarrow{k_2} \text{Fpg}\cdot(\text{DNA})_p$$

the concentration of E3Q EcFpg used in the MPE-Fe(II) footprinting experiments (Figure 3), the intensity of the overall footprint is diminished due to the larger amounts of reagent needed to observe DNA cleavage and the higher accessibility of the footprinting reagent. However, most notably, the hyperreactivity of the Sp nt is not observed under these conditions. A marginally increased amount of cleavage of the Sp nt (1.3-fold increased over the control with no protein) was observed when the amount of E3Q Fpg was quite high (100 nM). The extent of the footprinted region with Fe(II)-EDTA was also reduced compared to that of the Fe-EDTA reagent tethered to methidium (Figure 6). The more efficient cleavage of the Sp nt with MPE-Fe(II) suggests that an intercalation site is created upon binding of E3Q EcFpg to the Sp-containing duplex. However, since some hyperreactivity is observed at high EcFpg concentrations, the presence of EcFpg likely also distorts the Sp nt or alters its accessibility to increase its reactivity with hydroxyl radicals.

Fpg Catalyzes the Removal of Gh and Sp as Efficiently as OG. Under single-turnover conditions (STO) where [DNA] < [enzyme], we previously established that EcFpg excises OG, Gh, and Sp opposite all the four bases in the 18 bp duplex (*49*). To allow for comparison with the binding and footprinting experiments described herein, the kinetic properties with the 30 bp substrates containing Gh, Sp, and OG opposite all four natural bases were examined. In each case, the lesion-containing strand was end-labeled with ^{32}P-containing phosphate at the 5′-end, and the activity was assessed by the extent of strand scission at the lesion site as a function of time. EcFpg has previously been shown to catalyze both removal of OG and associated β- and δ-elimination reactions to provide strand scission at the lesion site (*57*). Importantly, quenching with NaOH gave observed rates for strand scission similar to those that had not been treated with base, indicating that intact abasic sites are not present in the reaction mixture under these conditions. This is consistent with tight association of the glycosylase and lyase functions of EcFpg. Using the kinetic approach and analysis reported previously (*49*), values for the rate constant k_2, encompassing all steps involving base excision (Scheme 1), were determined. It should be noted that a NaCl concentration of 30 mM was used in these experiments; however, rate constants for several substrates (Sp·G, OG·C, and OG·A) were also measured at 100 mM NaCl and similar results obtained.

Under STO conditions, with the 30 bp duplex at 37 °C, both Gh and Sp are excised opposite all four bases. The rates of excision of both Gh and Sp are similar to each other; however, the rate constants are much higher when compared to the corresponding rates with the 18 bp duplex (*49*). The net result is that in the 30 bp duplex sequence, the rate constants for EcFpg-catalyzed removal of Gh and Sp opposite C, G, and T are similar to those for removal of OG (Table 2). This is in contrast to a reduced rate of removal of Gh and Sp relative to OG in the corresponding 18 bp duplexes when paired with C, T, or G reported previously (*45*). For example, EcFpg-catalyzed removal of both Gh and Sp opposite C in the 30 bp duplex yielded rate constants of 21 ± 1 min^{-1}, a value that is similar to the value of 16 ± 2 min^{-1} observed for removal of OG from the corresponding OG·C base pair-containing duplex. Notably, the rate of removal of OG by EcFpg, opposite G, C, and T, does not seem to be as sensitive to duplex length,[3] as is the case with the Gh and Sp. The rates of excision of Gh from Gh·A base pairs (1.4 ± 0.2 min^{-1}) and Sp from Sp·A base pairs (1.5 ± 0.2 min^{-1}) in the 30 bp duplex are 5-fold higher than that observed for excision of OG from an OG·A base pair (0.27 ± 0.01 min^{-1}). However, the magnitude of the difference between Gh/Sp and OG in the longer duplex, when paired with A, is slightly smaller than with the 18 bp duplex since removal of OG opposite A is enhanced. The trend of preferred removal of Gh and Sp opposite C over A is also maintained. The increased efficiency of removal of Gh and Sp in the longer duplex sequence also results in a slightly increased rate of removal of both lesions opposite C relative to that opposite G. Somewhat surprisingly, however, is the fact that even in the longer duplex, the processing of Gh relative to Sp by EcFpg is remarkably similar despite major differences in the structures of the two hydantoins.

Table 2: Rate Constants (k_2) Determined for the Glycosylase Activity of EcFpg under Single-Turnover Conditions at 37 °C

central base pair[a]	k_2 (min^{-1})	central base pair[a]	k_2 (min^{-1})
OG·C	16 ± 2	OG·G	13 ± 1
Gh·C	21 ± 1	Gh·G	14 ± 1
Sp·C	21 ± 1	Sp·G	15 ± 1
OG·A	0.27 ± 0.01	OG·T	10 ± 1
Gh·A	1.4 ± 0.2	Gh·T	16 ± 1
Sp·A	1.5 ± 0.2	Sp·T	14 ± 1

[a] In 30-bp duplex (see methods).

DISCUSSION

Though seemingly deceptively simple, the excision of damaged bases mediated by BER glycosylases is a complex and multistep process (*58*, *59*). Minimally, this process requires initial recognition of the damaged base within duplex DNA, melting of the bp, extrusion of the damaged nucleotide from the helix, and stabilization of the appropriate extrahelical conformation for base cleavage (*58*). In the case of EcFpg, pre-steady state kinetic studies suggest that several transient enzyme substrate complexes must be formed prior to excision of the damaged base (*60*, *61*). The lesion-recognition complex (LRC) formed prior to base excision is represented by the structure of E3Q BsFpg bound to an OG·

[3] For reference, the relevant rate constants (k_2) for removal of OG from the OG·X base pair-containing 18 bp duplex under the same experimental conditions are as follows: 16 ± 2 min^{-1} for OG·C, 16 ± 1 min^{-1} for OG·T, 18 ± 1 min^{-1} for OG·G, and 0.05 ± 0.01 min^{-1} for OG·A.

C substrate (Figure 1B) (*44*). In the LRC, the extrahelical OG is lodged in the *syn* conformation in a large enzyme pocket. Though there are many OG contacts, the main feature not possible with G is a specific hydrogen bond with the carbonyl oxygen of Ser 220 of BsFpg with NH7 of OG. In addition, an important feature of the LRC (*44*), compared to other structures (*62*, *63*), was the closure and ordering of a flexible loop around the OG that provides several interactions of backbone amides with O6 of OG (*44*). Due to the structural similarities of Gh and Sp to OG, a similar recognition strategy for Fpg enzymes could be envisioned for these lesions (Figure 1). However, caution should be exercised in making such extensions since structural studies of *Lactococcus lactis* Fpg bound to carbocyclic FapydG-containing DNA revealed a recognition mode significantly different from that observed with OG even though FapydG is quite similar to OG (*64*). The flexibility to adopt alternate recognition complexes may be a feature that allows Fpg to recognize a wide variety of substrates.

To reveal features of recognition and binding unique to the hydantoin lesions separate from base excision, EMSA and footprinting experiments with the inactive variant, E3Q EcFpg, and duplexes containing Gh, Sp, and OG opposite both C and G were performed. An unexpected finding in the EMSA experiments with E3Q EcFpg binding to various lesion-containing duplexes was the higher affinity for the Gh- and Sp-containing duplexes over those containing OG. Indeed, E3Q EcFpg exhibits an affinity for the Gh- and Sp-containing duplexes at least 3 orders of magnitude higher than that for the corresponding OG-containing duplex. The higher affinity of E3Q EcFpg for the Gh- and Sp-containing duplexes may be related to the fact that Gh and Sp lesions are more destabilizing to the DNA duplex than OG as indicated by UV melting studies (*29*). The exact amount of destabilization caused by Gh and Sp relative to OG is highly dependent on the sequence and base pairing context, but generally, the observed T_m is reduced several degrees with both Gh and Sp. Molecular dynamics simulations also suggested that Sp would cause duplex distortion by affecting base stacking of the neighboring Watson−Crick base pairs (*65*). The reduced local stability of the duplex proximal to the Gh and Sp lesion sites may facilitate opening of the helix and disruption of the base pair. Reduced duplex stability caused by the presence of Gh- and Sp-containing base pairs may be further magnified upon binding of EcFpg. Recent structures of BsFpg forced to interrogate normal non-lesion-containing DNA via disulfide trapping suggest that Fpg actively tests the robustness of base pairs as part of the search process for DNA damage (*66*). In these structures, a phenylalanine residue (Phe 144) was found to intercalate at normal base pairs (G·C and A·T) which resulted in severe buckling of the base pair. Though buckled, the Watson−Crick base pairs remained intact; however, lesion-containing base pairs may more readily snap open when subjected to these conditions. Once they have been extruded, favorable interactions of the extruded base and the base opposite facilitate capture and excision of the damaged base. If similar hydrogen bonding interactions in the base-clipping pocket can be made with both OG and the hydantoin lesions, the more facile base pair disruption may make the overall affinity higher with the hydantoin lesion duplexes.

The substitution of Glu 3 with Gln in E3Q EcFpg that was made to inactivate the enzyme may also magnify the difference in binding between OG and the Gh and Sp lesion-containing duplexes. Glu 3 is located near the N-terminal proline (Pro 2) which is tucked into the active site to participate in the base displacement reaction (*57*). In the LRC structure, some small differences were observed at position 3 compared to WT BsFpg, and they prevent steric clashes caused by the presence of the amide -NH2 group of Gln 3 (*44*). In fact, the amide functionality of Gln 3 was observed in the LRC to hydrogen bond to the 8-oxo group of OG.

The binding data with E3Q EcFpg also show tighter binding with duplexes containing Sp opposite both C and G than the corresponding duplexes containing Gh. This may reflect both more facile disruption of Sp-containing base pairs and more favorable interactions of Sp within the active site of E3Q EcFpg. On the basis of its structure, Gh is likely more readily accommodated within the duplex and results in less local base pair distortion. If the Gh lesion adopts an enol tautomer, this provides a planar base heterocycle that would be even less disruptive to base stacking. In addition, the Gh lesion is positively charged, and this feature may provide for favorable interactions with the negatively charged DNA backbone.

The base opposite Gh and Sp also exerts a strong influence on the relative dissociation constants of E3Q EcFpg. The K_d values show that E3Q EcFpg binds more efficiently (200−400-fold) to the hydantoin lesions when paired with C over G. This may be expected since Fpg has been shown to prefer a pyrimidine opposite OG (*54*). In the structures of Fpg bound to DNA, there is an Arg that fills the void left after extrusion of OG and makes specific hydrogen bonds to C (*44*, *62*, *63*). The opposite base effect may also be a consequence of more stable base pairing of Gh and Sp with G over C such that the Gh/Sp·C bp is more easily disrupted and more readily recognized (*29*). In fact, both Gh and Sp can mimic "T", and thus, Gh_{syn} or Sp_{syn} can base pair with G in the same fashion as a T_{anti}·G_{anti} wobble pair (Figure 7) (*67*).

The high affinity of E3Q EcFpg for the Gh- and Sp-containing duplexes suggested that footprinting techniques would provide insight into the recognition features used by EcFpg with these unique lesions within the DNA. Indeed, footprinting using hydroxyl radicals produced from MPE-Fe(II) revealed that E3Q EcFpg provides an unusual pattern of protected nucleotides. The protected region is extensive, encompassing 15−16 nts and spans both strands of the duplex. This is in contrast to previous results with WT EcFpg bound to a product analogue duplex using Fe-EDTA hydroxyl radical footprinting where protection of a 5−6 nt span on the THF-containing strand was observed (*51*, *55*). The footprinting results with MPE-Fe(II) of E3Q Fpg and the hydantoin-containing duplexes also indicate a binding site that is approximately twice as large as what would be anticipated on the basis of the reported Fpg−DNA structures (*44*, *62*, *63*). The larger-than-expected footprint is due in part to the use of an intercalating footprinting reagent, as illustrated by the smaller footprint using the Fe(II)-EDTA reagent (Figure 6). The methidium moiety of the MPE-Fe-(II) reagent will be unable to intercalate if the protein disrupts the duplex structure or is only contacting one strand of the duplex. Moreover, duplex regions adjacent to the site bound

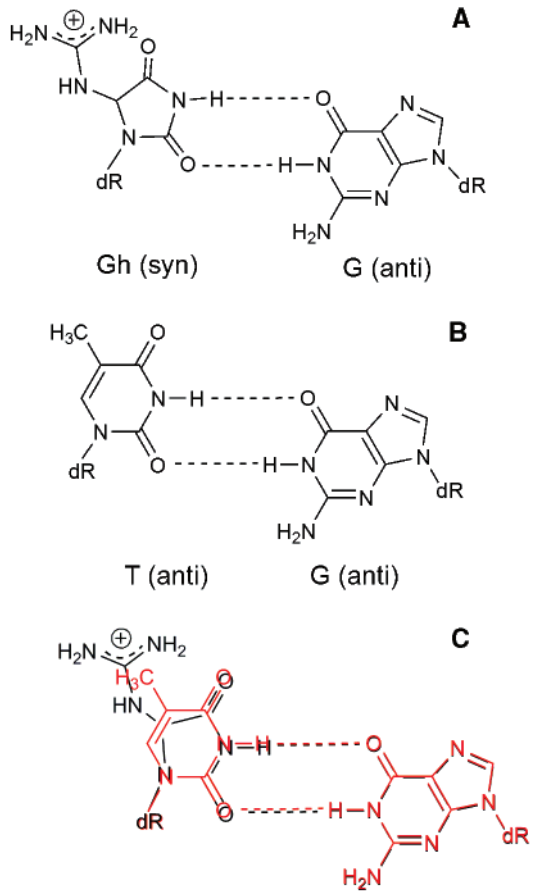

FIGURE 7: Proposed base pairing of Gh with G. (A) Proposed base pairing of Gh_{syn}·G_{anti}. (B) Wobble base pairing of T_{anti}·G_{anti}. (C) Overlay of the Gh_{syn}·G_{anti} base pair on the T_{anti}·G_{anti} base pair.

by E3Q EcFpg may be less able to open and unwind to accommodate methidium intercalation. The large footprint also reflects the unusual structural properties of the complex formed between E3Q EcFpg and the duplexes containing the Gh and Sp lesions. These results indicate that the structural features of these complexes are distinctly different from those of the corresponding complexes of Fpg with OG-containing and abasic site product or analogue-containing duplexes.

The most surprising result from the MPE-Fe(II) footprinting experiments was the observation that while the Gh nucleotide is protected from cleavage by E3Q EcFpg, the binding of E3Q EcFpg to the Sp-containing duplexes makes the Sp nucleotide hyperreactive to hydroxyl radical cleavage. Since MPE-Fe(II) contains an intercalating moiety, delivery of hydroxyl radicals to the vicinity of the Sp sugar likely requires the ability to intercalate at this site. This suggests that in the presence of Fpg, an intercalation site at the Sp nucleotide is created that can accommodate the methidium intercalator. Notably, intercalators often target sites that are more open or deformable, such as mismatched sites in DNA (*68*) or bulged and triple-base pair sites within RNA (*69*, *70*). The unusual spirocyclic structure of Sp may require that the helix be more open at this site; indeed, calculations suggest that in the Sp_{syn} conformation the steric bulk of Sp preferentially shifts the hydantoin ring to the major groove while making hydrogen bonds to G. The shift toward the exterior of the helix leads to less destabilization as a result of the Sp spirocycle (*65*, *71*). Moreover, when E3Q Fpg binds, the region at the Sp-containing base pair may be further altered to create an open base pair platform for the methidium intercalator. This is an unusual example of an intercalation site created by the binding of the DNA by a protein. This result is reminiscent of studies with TATA-binding protein (TBP) binding to TATA sequence-containing DNA which created a hot spot for intercalation and alkylation by the antibiotic pluramycin downstream of the TATA box (*72*). In this case, it was proposed that the binding of TBP to the TATA box caused transient unwinding on the 3′ side of the binding site that facilitated intercalation; moreover, the intercalation event stabilized the distorted DNA to provide for improved stability of the TBP−TATA complex. The specific recognition of the E3Q EcFpg−Sp-containing DNA duplex complex by MPE-Fe(II) also suggests a unique approach by which such protein−DNA complexes may be targeted by small molecules.

Though the binding studies indicate considerably more affinity of EcFpg for duplexes containing Gh and Sp over OG, the rates of base removal under single-turnover conditions are similar for all three lesions in the 30 bp duplex, when paired opposite C, G, or T. This may be due to specific interactions in the base recognition pocket that may be optimized to catalyze removal of OG. In the X-ray structure of the OG LRC (Figure 1), the ordering of the flexible loop (βF-α10) provides for a number of hydrogen bonding interactions of backbone amides with O6 of OG (*44*). These interactions were suggested to be important for stabilizing anion development at O6 of OG as the base is excised from the sugar. Though Gh and Sp may be accommodated within the base binding pocket, these damaged nucleotides may not be able to achieve the optimal catalytic conformation as readily as OG. Interestingly, a recent structure of a hOGG1 mutant engineered to partially obstruct the active site (Q315F hOGG1) in a complex with an OG·C duplex illustrated that despite the ability to place the OG base nearly completely into the active site, the mutant enzyme cannot catalyze OG excision (*73*). This suggests that another level of quality control used by BER glycosylases is perfect geometric alignment of the damaged nucleotide within the active site to achieve the optimal transition state for base cleavage. Additional pre-steady-state kinetic and structural studies of hydantoin lesions with Fpg and other glycosylases would be exceedingly valuable in further testing these hypotheses.

An important next step will be to determine how the unique features of recognition and removal of the hydantoin lesions by repair enzymes impact their mutagenic potential in cells. For example, the high affinity of Fpg for the hydantoin lesions *may* translate into location and excision in a cellular context that are more efficient than that of OG. Capture of Gh and Sp lesions by repair enzymes prior to replication would be expected to prevent mutagenesis. However, the strong miscoding properties of Gh and Sp lesions may be further exacerbated by attempts to repair these lesions in the inappropriate base pairing context. Specifically, the presence of G → C transversion mutations is consistent with the transient formation of Gh·G and Sp·G pairs (*34*). Removal of the lesion from a Gh·G or Sp·G base pair would enhance mutagenesis mediated by these lesions. Removal of all lesions (OG, Gh, and Sp) opposite A is significantly less efficient than opposite any of the other bases, consistent with a recognition feature that selects against A (*45*, *49*).

However, EcFpg removes the hydantoin lesions Gh and Sp *more efficiently* than OG when in a base pairing context with A. In the case of OG, removal of misincorporated adenines is performed by *E. coli* MutY; however, the MutY glycosylase does not remove adenine from Gh·A or Sp·A base pairs to an appreciable extent (*49*). Recently, the presence of MutY was shown to reduce the bypass efficiency of Gh and Sp lesions in vivo, suggesting that MutY may intercept Gh/Sp·A bps and prevent their propagation, thereby mitigating some of their genotoxic properties (*35*). Clearly lesion recognition and repair are important modifiers of the mutagenesis and toxicity of hydantoin lesions. Further work evaluating the mutagenic potential of Gh and Sp in cellular assays with different repair capabilities may provide interesting connections between properties of these lesions and specific steps in the repair process, as well as further elaborate how these unique lesions contribute to oxidative stress-mediated mutagenesis.

ACKNOWLEDGMENT

The pKK-Fapy2 plasmid used for overexpression of WT EcFpg was provided by Dr. Mark Michaels and Dr. Jeffrey Miller (University of California, Los Angeles, CA). We thank Dr. Micheal Leipold for making the pKKE3Q plasmid vector for overexpression of E3Q Fpg. ESI-MS was supported in part by the National Science Foundation (CHE-9798413). DNA sequencing was performed by the sequencing facility in the University of Utah Medical School, which is supported in part by National Institutes of Health (NCI) Grant 5P30CA43014.

REFERENCES

1. Henle, E. S., and Linn, S. (1997) Formation, prevention and repair of DNA damage by iron/hydrogen peroxide, *J. Biol. Chem. 272*, 19095−19098.
2. Frenkel, K. (1992) Carcinogen-Mediated Oxidant Formation and Oxidative DNA Damage, *Pharmacol. Ther. 53*, 127−166.
3. Bjelland, S., and Seeberg, E. (2003) Mutagenicity, toxicity and repair of DNA base damage induced by oxidation, *Mutat. Res. 531*, 37−80.
4. Beckman, K. B., and Ames, B. N. (1997) Oxidative decay of DNA, *J. Biol. Chem. 272*, 19633−19636.
5. Kamiya, H. (2003) Mutagenic potentials of damaged nucleic acids produced by reactive oxygen/nitrogen species: Approaches using synthetic oligonucleotides and nucleotides, *Nucleic Acids Res. 31*, 517−531.
6. Lindahl, T., and Wood, R. D. (1999) Quality control by DNA repair, *Science 286*, 1897−1905.
7. Friedberg, E. C., Walker, G. C., and Seide, W. (1995) *DNA Repair and Mutagenesis*, ASM Press, Washington, DC.
8. Schärer, O. D. (2003) Chemistry and Biology of DNA Repair, *Angew. Chem., Int. Ed. 42*, 2946−2974.
9. Barnes, D. E., and Lindahl, T. (2004) Repair and genetic consequences of endogenous DNA base damage in mammalian cells, *Annu. Rev. Genet. 38*, 445−476.
10. Al-Tassan, N., Chmiel, N. H., Maynard, J., Fleming, N., Livingston, A. L., Williams, G. T., Hodges, A. K., Davies, D. R., David, S. S., Sampson, J. R., and Cheadle, J. P. (2002) Inherited variants of MYH associated with somatic G:C to T:A mutations in colorectal tumors, *Nat. Genet. 30*, 227−232.
11. Ames, B. N., Shigenaga, M. K., and Hagen, T. M. (1993) Oxidants, antioxidants, and the degenerative diseases of aging, *Proc. Natl. Acad. Sci. U.S.A. 90*, 7915−7922.
12. Ames, B. N., and Gold, L. S. (1991) Endogenous mutagens and the causes of aging and cancer, *Mutat. Res. 250*, 121.
13. Hoeijmakers, J. H. J. (2001) Genome maintanence mechanisms for preventing cancer, *Nature 411*, 366−374.
14. Lindahl, T. (1993) Instability and decay of the primary structure of DNA, *Nature 362*, 709−715.
15. Cadet, J., Delatour, T. T. D., Gasparutto, D., Pouget, J. P., Ravanat, J. L., and Sauvaigo, S. (1999) Hydroxyl radicals and DNA damage, *Mutat. Res. 424*, 9−21.
16. Neeley, W. L., and Essigmann, J. M. (2006) Mechanisms of formation, genotoxicity, and mutation of guanine oxidation products, *Chem. Res. Toxicol. 19*, 491−505.
17. Luo, W., Muller, J. G., Rachlin, E. M., and Burrows, C. J. (2000) Characterization of spiroiminodihydantoin as a product of one-electron oxidation of 8-oxo-7,8-dihydroguanosine, *Org. Lett. 2*, 613−616.
18. Luo, W., Muller, J. G., Rachlin, E. M., and Burrows, C. J. (2001) Characterization of hydantoin products from one-electron oxidation of 8-oxo-7,8-dihydroguanosine in a nucleoside model, *Chem. Res. Toxicol. 14*, 927−938.
19. Ye, Y., Muller, J. G., Luo, W., Mayne, C. L., Shallop, A. J., Jones, R. A., and Burrows, C. J. (2003) Formation of ^{13}C, ^{15}N, ^{18}O-labeled guanidinohydantoin from guanosine oxidation with singlet oxygen. Implications in structure and mechanism, *J. Am. Chem. Soc. 125*, 13926−13927.
20. Ravanat, J. L., Saint-Pierre, C., Di Mascio, P., Martinez, G. R., Medeiros, M. H. G., and Cadet, J. (2001) Damage of isolated DNA mediated by singlet oxygen, *Helv. Chim. Acta 84*, 13926−13927.
21. Luo, W., Muller, J. G., and Burrows, C. J. (2001) The pH-dependent role of superoxide in riboflavin-catalyzed photooxidation of 8-oxo-7,8-dihydroguanosine, *Org. Lett. 3*, 2801−2804.
22. Misiaszek, R., Crean, C., Joffe, A., Geacintov, N. E., and Shafirovich, V. (2004) Oxidative DNA damage associated with combination of guanine and superoxide radicals and repair mechanisms via radical trapping, *J. Biol. Chem. 279*, 32106−32115.
23. Sugden, K. D., Campco, C. K., and Martin, B. D. (2001) Direct oxidation of guanine and 7,8-dihydro-8-oxoguanosine in DNA by high-valent chromium complex: A possible mechanism for chromate genotoxicity, *Chem. Res. Toxicol. 14*, 1315−22.
24. Slade, P. G., Hailer, M. K., Martin, B. D., and Sugden, K. D. (2005) Guanine-specific oxidation of double stranded DNA by Cr(VI) and ascorbic acid forms spiroiminodihydantoin and 8-oxo-2′deoxyguanosine, *Chem. Res. Toxicol. 18*, 1140−1149.
25. Niles, J. C., Burney, S., Singh, S. P., Wishnok, J. S., and Tannenbaum, S. R. (1999) Peroxynitrite reaction products of 3′,5′-di-O-acetyl-8-oxo-7,8-dihydro-2′-deoxyguanosine, *Proc. Natl. Acad. Sci. U.S.A. 96*, 11729−11734.
26. Niles, J. C., Wishnok, J. S., and Tannenbaum, S. R. (2001) Spiroiminodihydantoin is the major product of the 8-oxo-7,8-dihydroguanosine reaction with peroxynitrite in the presence of thiols and guanosine photooxidation by methylene blue, *Org. Lett. 3*, 963−966.
27. Niles, J. C., Wishnok, J. S., and Tannenbaum, S. R. (2004) Spiroiminodihydantoin and guanidinohydantoin are the dominant products of 8-oxoguanosine oxidation at low fluxes of peroxynitrite: Mechanistic studies with ^{18}O, *Chem. Res. Toxicol. 17*, 1510−1519.
28. Hailer, M. K., Slade, P. G., Martin, B. D., and Sugden, K. D. (2005) Nei deficient *Escherichia coli* are sensitive to chromate and accumulate the oxidized guanine lesion spiroiminodihydantoin, *Chem. Res. Toxicol. 18*, 1378−1383.
29. Kornyushyna, O., Berges, A. M., Muller, J. G., and Burrows, C. J. (2002) In vitro nucleotide misinsertion opposite the oxidized guanosine lesions spiroiminodihydantoin and guanidinohydantoin and DNA synthesis past the lesions using *Escherichia coli* DNA polymerase I (Klenow fragment), *Biochemistry 41*, 15304−15314.
30. Kornyushyna, O., and Burrows, C. J. (2003) Effect of the oxidized lesions spiroiminodihydantoin and guanidinohydantoin on proofreading by *Escherichia coli* DNA polymerase I (Klenow Fragment) in different sequence contexts, *Biochemistry 42*, 13008−13018.
31. Shibutani, S., Takeshita, M., and Grollman, A. P. (1991) Insertion of specific bases during DNA synthesis past the oxidtion-damaged base 8-oxodG, *Nature 349*, 431−434.
32. Grollmann, A. P., and Moriya, M. (1993) Mutagenesis by 8-oxoguanine: An enemy within, *Trends Genet. 9*, 246−249.
33. Wood, M. L., Esteve, A., Morningstar, M. L., Kuziemko, G. M., and Essigmann, J. M. (1992) Genetic effects of oxidative DNA damage: Comparative mutagenesis of 7,8-dihydro-8-oxoguanine and 7,8-dihydro-8-oxoadenine in *Escherichia coli*, *Nucleic Acids Res. 20*, 6023−6032.
34. Henderson, P. T., Delaney, J. C., Muller, J. G., Neeley, W. L., Tannenbaum, S. R., Burrows, C. J., and Essigmann, J. M. (2003)

The hydantoin lesions from oxidation of 7,8-dihydro-8-oxoguanine are potent sources of replication errors in vivo, *Biochemistry 42*, 9257−9262.
35. Delaney, S., Neeley, W. L., Delaney, J. C., and Essigman, J. M. (2007) The Substrate Specificity of MutY for Hyperoxidized Guanine Lesions in Vivo, *Biochemistry 46*, 1448−1455.
36. Michaels, M. L., Cruz, C., Grollman, A. P., and Miller, J. H. (1992) Evidence that MutY and MutM combine to prevent mutations by an oxidatively damaged form of guanine in DNA, *Proc. Natl. Acad. Sci. U.S.A. 89*, 7022−7025.
37. Michaels, M. L., Tchou, J., Grollman, A. P., and Miller, J. H. (1992) A repair system for 8-oxo-7,8-dihydroguanine, *Biochemistry 31*, 10964−10968.
38. Tajiri, T., Maki, H., and Sekiguchi, M. (1995) Functional cooperation of MutT, MutM and MutY proteins in preventing mutations casued by spontaneous oxidation of guanine nucleotide in *Escherichia coli*, *Mutat. Res. 336*, 257−267.
39. Krokan, H. E., Standal, R., and Slupphaug, G. (1997) DNA glycosylases in the base excision repair of DNA, *Biochem. J. 325*, 1−16.
40. David, S. S., and Williams, S. D. (1998) Chemistry of glycosylases and endonucleases involved in base-excision repair, *Chem. Rev. 98*, 1221−1261.
41. Parikh, S. S., Mol, C. D., and Tainer, J. A. (1997) Base excision repair family portrait: Integrating the structure and chemistry of an entire DNA repair pathway, *Structure 5*, 1543−1550.
42. Fromme, J. C., Banerjee, A., and Verdine, G. L. (2004) DNA glycosylase recognition and catalysis, *Curr. Opin. Struct. Biol. 14*, 43−49.
43. Fromme, J. C., and Verdine, G. L. (2004) Base Excision Repair, *Adv. Protein Chem. 69*, 1−41.
44. Fromme, C. J., and Verdine, G. L. (2003) DNA lesion recognition by the bacterial repair enzyme MutM, *J. Biol. Chem. 278*, 51543−51548.
45. Leipold, M. D., Workman, H., Muller, J. G., Burrows, C. J., and David, S. S. (2003) Recognition and removal of oxidized guanines in duplex DNA by the base excision repair enzymes hOGG1, yOGG1, and yOGG2, *Biochemistry 42*, 11373−11381.
46. Hazra, T. K., Muller, J. G., Manuel, R. C., Burrows, C. J., Lloyd, R. S., and Mitra, S. (2001) Repair of hydantoins, one electron oxidation product of 8-oxoguanine, by DNA glycosylases of *Escherichia coli*, *Nucleic Acids Res. 29*, 1967−1974.
47. Hailer, M. K., Slade, P. G., Martin, B. D., Rosenquist, T. A., and Sugden, K. D. (2005) Recognition of the oxidized lesions spiroiminodihydantoin and guanidinohydantoin in DNA by the mammalian base excision repair glycosylases NEIL1 and NEIL2, *DNA Repair 4*, 41−50.
48. Michaels, M. L., Pham, L., Cruz, C., and Miller, J. H. (1991) MutM, a protein that prevents G-C to T-A transversions, is formamidopyrmidine-DNA glycosylase, *Nucleic Acids Res. 19*, 3629−3632.
49. Leipold, M. D., Muller, J. G., Burrows, C. J., and David, S. S. (2000) Removal of hydantoin products of 8-oxoguanine oxidation by the *Escherichia coli* DNA repair enzyme, Fpg, *Biochemistry 39*, 14984−14992.
50. Porello, S. L., Williams, S. D., Kuhn, H., Michaels, M. L., and David, S. S. (1996) Specific recognition of substrate analogs by the DNA mismatch repair enzyme MutY, *J. Am. Chem. Soc. 118*, 10684−10692.
51. Tchou, J., Michaels, M. L., Miller, J. H., and Grollman, A. P. (1993) Function of the Zinc finger in *Escherichia coli* Fpg protein, *J. Biol. Chem. 268*, 26738−26744.
52. Tchou, J., Bodepudi, V., Shibutani, S., Antoscheckin, I., Miller, J., Grollman, A. P., and Johnson, F. P. (1994) Substrate Specificity of Fpg Protein, *J. Biol. Chem. 269*, 15318−15324.
53. Zaika, E. I., Perlow, R. A., Matz, E., Broyde, S., Gilboa, R., Grollman, A. P., and Zharkov, D. O. (2004) Substrate Discrimination by Formamidopyrimidine-DNA Glycosylase, *J. Biol. Chem. 279*, 4849−4861.
54. Castaing, B., Geiger, A., Seliger, H., Nehls, P., Laval, J., Zelwer, C., and Boiteux, S. (1993) Cleavage and binding of a DNA fragment containing a single 8-oxoguanine by wild type and mutant FPG proteins, *Nucleic Acids Res. 21*, 2899−2905.
55. Castaing, B., Fourrey, J. L., Hervouet, N., Thomas, M., Boiteux, S., and Zelwer, C. (1999) AP site structural determinants for Fpg specific recognition, *Nucleic Acids Res. 27* (2), 608−615.
56. Maxam, A. M., and Gilbert, W. (1980) Sequencing end-labeled DNA with base specific chemical cleavages, *Methods Enzymol. 65*, 499−560.
57. Zharkov, D. O., Rieger, R. A., Iden, C. R., and Grollman, A. P. (1997) NH_2-terminal proline acts as a nucleophile in the glycosylase/AP-lyase reaction catalyzed by *Escherichia coli* formamidopyrimidine-DNA glycosylase (Fpg) protein, *J. Biol. Chem. 272*, 5335−5341.
58. Stivers, J. T. (2004) Site-Specific DNA Damage Recognition by Enzyme-Induced Base Flipping, *Prog. Nucleic Acid Res. Mol. Biol. 77*, 37−65.
59. Hitomi, K., Iwai, S., and Tainer, J. A. (2007) The intricate structural chemistry of base excision repair machinery: Implications for DNA damage recognition, removal and repair, *DNA Repair* (2007) *6*, 410-428.
60. Koval, V. V., Kuznetsov, N. A., Zharkov, D. O., Ishchenko, A. A., Douglas, K. T., Nevinsky, G. A., and Federova, O. S. (2004) Pre-steady-state kinetics shows differences in processing of various DNA lesions by *Escherichia coli* formamidopyrimidine-DNA glycosylase, *Nucleic Acids Res. 32*, 926−935.
61. Kuznetsov, N. A., Koval, V. V., Zharkov, D. O., Vorobjev, Y. N., Nevinsky, G. A., Douglas, K. T., and Fedorova, O. S. (2007) Pre-Steady-State Kinetic Study of Substrate Specificity of *Escherichia coli* Formamidopyrimidine-DNA Glycosylase, *Biochemistry 46*, 424−435.
62. Fromme, C. J., and Verdine, G. L. (2002) Structural insights into lesion recognition and repair by the bacterial 8-oxoguanine DNA glycosylase Mut M, *Nat. Struct. Biol. 9*, 544−552.
63. Gilboa, R., Zharkov, D. O., Golan, G., Fernandes, A. S., Gerchman, S. E., Matz, E., Kycia, J., Grollman, A. P., and Shoham, G. (2002) Structure of formamidopyrimidine-DNA glycosylase covalently complexed to DNA, *J. Biol. Chem. 277*, 19811−19816.
64. Coste, F., Ober, M., Carell, T., Boiteux, S., Zelwer, C., and Castaing, B. (2004) Structural Basis for the Recognition of the FapydG Lesion (2,6-Diamino-4-hydroxy-5-formamidopyrimidine) by Formamidopyrimidine-DNA Glycosylase, *J. Biol. Chem. 279*, 44074−44083.
65. Jia, L., Shafirovich, V., Shapiro, R., Geacintov, N. E., and Broyde, S. (2005) Structural and thermodynamic features of spiroiminodihydantoin damaged DNA duplexes, *Biochemistry 44*, 13342−13353.
66. Banerjee, A., Santos, W. L., and Verdine, G. L. (2006) Structure of a DNA Glycosylase Searching for Lesions, *Science 311*, 1153−1157.
67. Zhao, X., Muller, J. G., Halasyam, M., David, S. S., and Burrows, C. J. (2007) In vitro ligation of oligodeoxynucleotides containing C8-oxidized purine lesions using bacteriophage T4 DNA ligase, *Biochemistry 46*, 3734−3744.
68. Junicke, H., Hart, J. R., Kisko, J., Giebov, O., Kirsch, I. R., and Barton, J. K. (2003) A rhodium(III) complex for high-affinity DNA base-pair mismatch recognition, *Proc. Natl. Acad. Sci. U.S.A. 100*, 3737−3742.
69. Chow, C. S., and Barton, J. K. (1992) Transition Metal complexes as probes of nucleic acids, *Methods Enzymol. 212*, 219−242.
70. Carlson, C. B., Vuyisich, M., Gooch, B. D., and Beal, P. A. (2003) Preferred RNA binding sites for a threading intercalator revealed by in vitro evolution, *Chem. Biol. 7*, 663−672.
71. Jia, L., Shafirovich, V., Shapiro, R., Geacintov, N. E., and Broyde, S. (2005) Spiroiminodihydantoin lesions derived from guanine oxidation, *Biochemistry 44*, 6043−6051.
72. Sun, D., and Hurley, L. H. (1995) TBP binding to the TATA box induces a specific downstream unwinding site that is targeted by pluramycin, *Chem. Biol. 2*, 457−469.
73. Radom, C. T., Banerjee, A., and Verdine, G. L. (2007) Structural characterization of human 8-oxoguanine DNA glycosylase variants bearing active site mutations, *J. Biol. Chem. 282*, 9182−9194.

BI602459V